PCCP

ELECTRONIC STRUCTURE OF P-TYPE PERYLENE MONOIMIDE -BASED DONOR–ACCEPTOR DYES ON THE NICKEL OXIDE (100) SURFACE: A DFT APPROACH

Journal:	*Physical Chemistry Chemical Physics*
Manuscript ID	CP-ART-04-2016-002510
Article Type:	Paper
Date Submitted by the Author:	14-Apr-2016

Complete List of Authors:	Kontkanen, Outi; Tampere University of Tehcnology, Department of Chemistry and Bioengineering; Tampere University of Technology, Department of Physics Niskanen, Mika; Tampere University of Technology, Department of Chemistry and Bioengineering Hukka, Terttu; Tampere University of Technology, Dept. of Chemistry and Bioengineering Rantala, Tapio; Tampere University of Technology, Department of Physics

ELECTRONIC STRUCTURE OF P-TYPE PERYLENE MONOIMIDE - BASED DONOR–ACCEPTOR DYES ON THE NICKEL OXIDE (100) SURFACE: A DFT APPROACH

O. V. Kontkanen,[a,b] M. Niskanen,[a,c*] T. I. Hukka[a*] and T. T. Rantala[b]

[a]Department of Chemistry and Bioengineering, Tampere University of Technology, P.O. Box 541, Tampere, FI-33101, FINLAND

[b]Department of Physics, Tampere University of Technology, P.O. Box 692, Tampere, FI-33101, FINLAND

[c]Department of Physics, Imperial College London, South Kensington Campus, London SW7 2AZ, U.K.

ABSTRACT

A p-type dye-sensitized solar cell, where the dye injects a hole to the semiconductor, could be combined with typical Grätzel cell to create an efficient tandem device. However, the current p-type devices suffer from low efficiency. Here, geometries and electronic structures of four perylenemonoimide-based dyes (**1**–**4**) both as free and adsorbed on the NiO (100) semiconductor surface have been investigated to gain better understanding of the p-type devices. In particular, the electronic transitions relevant to charge transfer between the dye and the surface have been identified. Excitations have been evaluated by using the time dependent DFT calculations and the roles of frontier orbitals and band edges in transitions have been assessed. The adsorbed dyes can take either upright or slightly tilted geometries depending on the structure of the anchoring group and the binding mode of the dye. The adsorption slightly lowers the NiO band gap, from 4.06 eV to 3.90–3.96 eV depending on the surface–adsorbate system, and the band gaps of the dye molecules by 0.1–0.2 eV. Additionally, the adsorption mode of dye **1** moves the LUMO+1 level down by 0.5 eV. The effective mass of the charge carrier holes is significantly smaller at the NiO surface than in the bulk indicating the importance of the surface conductivity. We also found that the potential drop, i.e. the driving force for charge transfer from NiO to dye molecule depends on the adsorption mode of **1**.

keywords: DFT, TDDFT, perylenemonoimide, p-type, dye-sensitized, solar cells, nickel oxide, NiO (100) surface, HOMO–LUMO gap, band gap, density of states, electron transfer.

1. INTRODUCTION

Photovoltaics is one of the fastest growing technologies for generating renewable energy. Silicon-based solar cells, although widely used, are still costly. [1] Dye-sensitized solar cells (DSSC), offer attractive alternatives as inexpensive and light-weight devices, which perform well also in diffuse sunlight. [1,2] The currently known DSSCs are, however, less efficient than the silicon solar cells. [3] The n-type DSSCs, discovered in 1991 and known as Grätzel cells, have been studied the most. [4] The p-type DSSCs, have been studied much less, most probably because they have lower power conversion efficiencies (PCEs). For comparison, the PCEs of n-type DSSCs have reached 12–13 % [5,6] whereas those of the p-type DSSCs are presently 0.5–2.5 % [2,7–9].

Worth of attention about the n- and p-DSSCs is that they can be incorporated into a tandem cell (i.e. a pn-DSSC). The tandem construction enables collecting the sunlight at a wider spectral range and producing a larger open circuit voltage (V_{oc}) compared to either the n- or p-type DSSC alone. The theoretical maximum PCE of a tandem cell is over 40 % [10] while that of a single-junction silicon solar cell is 29 % [11], which makes the structure of a tandem-DSSC ideal to be pursued. The components of a pn-DSSC are the n- and p-type dyes, two semiconductors (e.g. NiO and TiO_2), and the electrolyte (e.g. I^-/I_3^-), which are connected in series inside a circuit. Although the V_{oc} increases in a pn-DSSC, the current flow through the cell is limited by the weakest performing component which is the p-type side of the cell. [12–14] Because of the low PCEs of the p-DSSCs an efficient pn-DSSC has not yet been realized.

A p-DSSC functions complementary to the n-DSSC. When the dye molecule in p-DSSC is excited, typically the excitation is followed by an electron transfer to the acceptor part of the dye further away from the semiconductor surface. Next, the hole left behind can transfer to the semiconductor. The electron on the acceptor part of the dye transfers to the electrolyte. Several p-type dyes have been experimentally studied in p-type DSSCs including perylene monoimide (PMI) derivatives in this study [2,6–9,15]. Typical dye-related problems have been linked to both the properties of orbitals (their locations and energy levels) and the (other) fast charge transfer

reactions competing with the intended charge transfer from the dye molecule to the semiconductor. [16,17] The most preferable dyes in general are of the donor-acceptor (D–A) type because they can be modified by synthetic means to reach the desirable electron transfer routes. In the D–A systems light excites the electron in the donor to be transferred to the acceptor. This separation of charges makes recombination slower. [18] It is desirable that the highest occupied molecular orbital (HOMO) of the dye has spatial overlap with the orbitals that make the valence band of the semiconductor to facilitate the hole transfer from the dye to the semiconductor. [3] Moreover, in p-DSSCs the valence bands of the semiconductor should locate energetically above the HOMO of the dye molecule in order to enable a fluent charge flow. The anchor group is also important especially if the anchor unit is conjugated throughout from the donor down to the surface, as conjugation may increase the charge transfer.

Experimental studies have indicated that NiO is not the most optimal choice for a semiconductor carrier of the p-type dyes because of its shallow valence band and low mobility of the holes. [3] However, the other alternatives, such as cubric oxide (CuO) and $CuAlO_2$ delafossite [19–21], so far, have lower photocurrents than NiO which leaves NiO the best choice at the present. However, changing the redox mediator from I^-/I_3^- into $Fe^{III/II}$ or $Co^{III/II}$ complex greatly enhances the open circuit voltage up to 645 mV [9] or 709 mV [22], respectively. Different electrode materials, such as fluorine-doped tin oxide (FTO) or platinum [23] have been tested, as well. Furthermore, the experimental studies of the p-type dyes [3, 17] indicate that the competing electron transfer reactions are fast compared to the current generating electron transfer in p-type DSSCs, meaning that recombination may take place before the charge reaches the semiconductor and the current flow is hindered. Besides, it is not yet known, if the mobility of charge carriers is higher at the surface or in the bulk of NiO.

The properties of NiO semiconductor are challenging to calculate, starting from the band gap. Experimental and theoretical band gaps of the NiO (100) surface have been reviewed in Table SI1. We are aware of previous modeling studies, where dye molecules, coumarin [24], porphyrin [25], diketopyrrolopyrrole derivatives [26], and ruthenium complexes [27] on the NiO (100) surface are examined. Additionally, one of the dye molecules studied in this article has been previously examined in vacuum at the PBE/6-31G(d) level of theory [15].

The aim of this work has been to gain a better atomic level understanding of the p-type devices. We have determined the minimum energy geometries and the electronic structures of four PMI-based, p-type donor–acceptor (D–A) dyes and studied their interactions with the NiO (100) semiconductor surface. [7,12,14] Additionally, we have determined the energy levels relevant to the electronic excitations and charge transfer reactions. Because NiO is known to be ionic and it has an antiferromagnetic (AF_2) order, we have taken spin-polarization into account in the calculations. [28,29]

2. COMPUTATIONAL MODELS AND METHODS

2.1 Models

Free dye molecules. Molecular models of the p-type donor–acceptor dyes, each derivative of perylenemonoimide (PMI), were built (Fig. 1). In one model (**1**) oligothiophene-trisphenylamine (TPA) moiety acts a donor and PMI as an acceptor. In the three other models PMI acts as a donor, and one of the following three moieties can act as an acceptor: naphthalene diimide without a phenyl bridge (NDI) in **2**, naphthalene diimide with a phenyl bridge (PhNDI) in **3**, and fullerene with a phenyl bridge (PhC_{60}) in **4**.

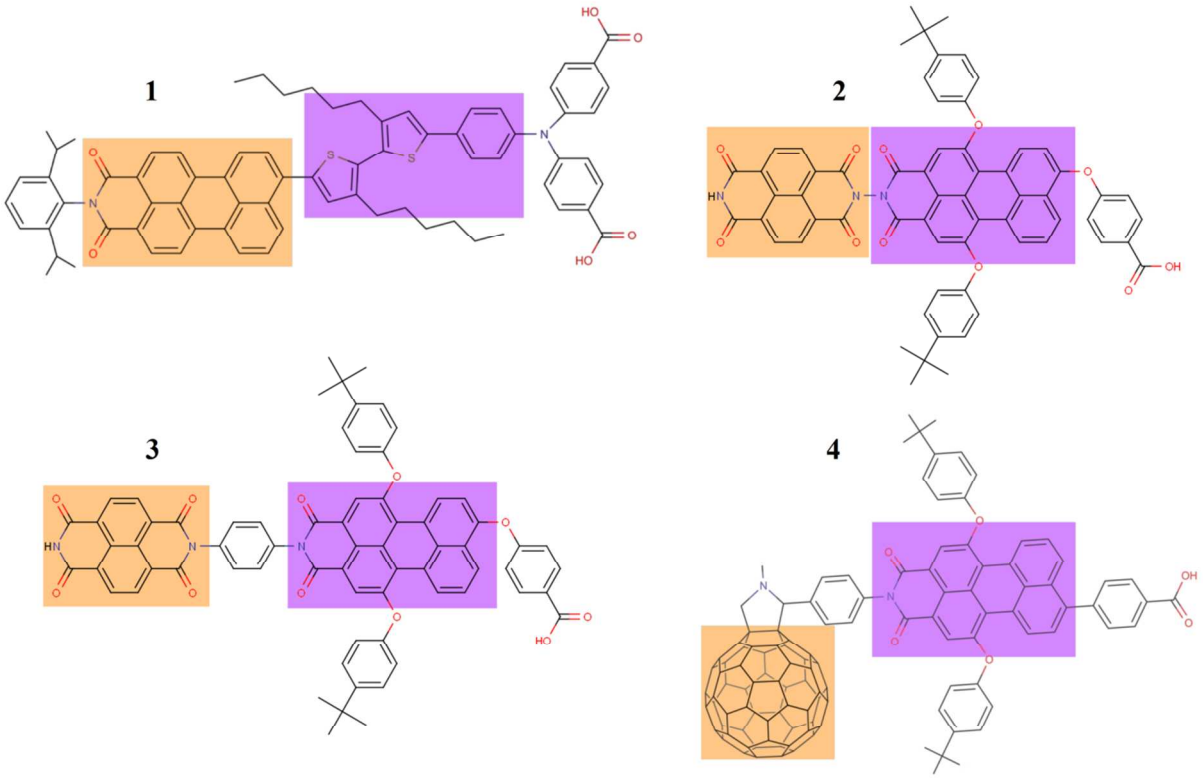

Fig. 1. Models of the p-type D–A dye molecules. The donors are purple and the acceptors are orange.

Semiconductor. The rock salt crystal structure of the p-type [28] NiO semiconductor with the cubic lattice constant a_0 of 4.176 Å [15,30] was used to construct the defect-free periodic 3D model of NiO. Typically a primitive unit cell containing two atoms is enough for optimization of the rock salt crystal structure. However, because the antiferromagnetism was taken into account, a supercell containing two Ni and two O atoms was used for the optimization of the lattice constant yielding an a_0 of 4.213 Å. The model of the NiO (100) surface (Fig. 2a), a 2D slab, was cut out from the optimized, periodic NiO bulk model as a four (4) layers thick 4×4 supercell. We choose to utilize the (100) surface because it is known to be the most stable, and therefore, most abundant of the NiO surfaces. Other surfaces like (110) or (111) tend to facet to surfaces containing (100) planes in order to minimize the surface energy, if not stabilized by defects or polar liquids or other external effects. [31] The center-to-center distance of the 2D slabs was 500Å in the "nonperiodic" direction. All atoms of the surface model were relaxed while keeping

the lattice constant frozen at optimized bulk value. The orientations of the spins in the surface model are visualized in Fig. 2b.

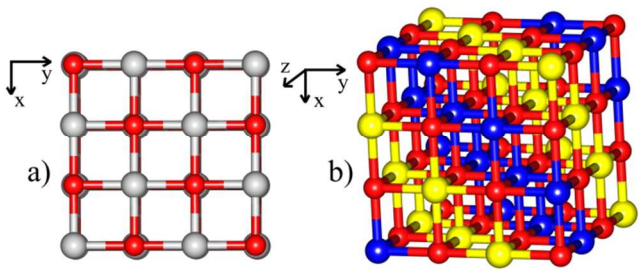

Fig. 2. (a) A sample 2 × 2 supercell of the NiO (100) surface slab and (b) the spin orientations in the structure: Ni spin up (yellow), Ni spin down (blue). Oxygen atoms are red.

Dye molecule adsorbed on the surface. First, the carboxylic acid groups of the dyes were anchored via covalent bonding (i.e. chemisorbed) on the four (4) layers thick NiO (100) surface slab. The acid groups are deprotonated in chemisorption and the released protons are bound on oxygen atoms of the NiO surface. Model **1** has two carboxylic acid groups which allow the anchoring via either a) one group or b) both carboxylic acid groups (Fig. 3a and 3b, respectively). Models **2**–**4** have only one anchoring group each (Fig. 3c–3e). The systems were relaxed to reach the minimum energy structures while keeping the lattice vectors frozen. Second, the rest of the dye molecules were added and bound to the anchor groups and relaxed. The geometries of **3** and **4** turned out to be more challenging to optimize than those of **1** and **2.** However, because the donor moieties and the carboxyphenoxy anchor units of **2** and **3** are the same, and the donor of **4** is the same as in **2**, we will be able to infer some expected behavior for the combined systems of **3** and **4**. Additionally, models for examining dye-dye-interactions were made based on the combined model. For these, the surface in the combined model was removed and the dye geometry relaxed while keeping the lattice vectors frozen.

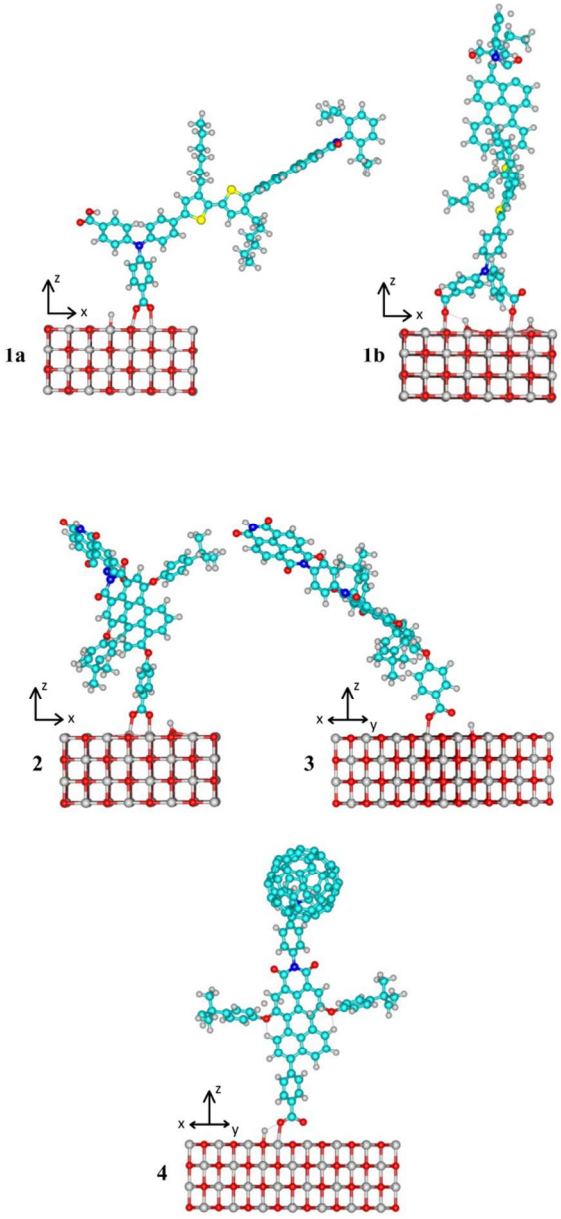

Fig. 3. The combined systems. Dye in model **1a** connects through one anchor whereas in **1b** it utilizes both anchoring groups. Combined systems **1** and **2** have optimized structures.

2.2 Methods

Preliminary optimizations with DFT and the following time-dependent DFT (TDDFT) calculations of the free dye molecules in vacuum were carried out using the Gaussian 09 program [32]. The global hybrid functional, B3LYP, [33,34,35] and the 6-31(d) basis set were used to optimize the ground state geometries and to calculate the vibrational frequencies with

DFT and the electronic transitions between the ground and excited states with TDDFT. The absence of the imaginary frequencies ensured the minimum energy structures. Molecular orbital energies and electronic excitations were calculated in order to examine possible charge transfer properties.

The free, pre-optimized dye molecules, the separate NiO bulk and the NiO (100) surface, as well as the combined 'dye adsorbed on the NiO (100)' -system were studied using DFT with the CRYSTAL09 [36,37] program. The B3LYP functional was used also in these calculations. The TZVP [38] basis set was chosen for molecule **1**, 6-31G(d,p) [39] for molecules **2-4**, and basis sets with contractions 86411/6411/41 and 8411/411 [40] for surface Ni and O, respectively. Because NiO is antiferromagnetic special convergence and spin-related tools were used for its modeling (for further details, see ESI).

The effective hole masses,

$$m^* = \frac{\hbar^2}{\frac{d^2E}{dk^2}}, \qquad (1)$$

were calculated for the hole transport properties and compared to the experimental value of $0.8m_0$ [41]. The m* is inversely proportional to the hole mobility. The equation (1) was used for calculating the effective masses, where $E(k)$ is the band energy as a function of wavevector k in that band (see band Figures below) and ħ is the reduced Planck constant.

We also calculated the adsorption energy,

$$E_{ads} = E_{D/NiO} - E_D - E_{NiO} \qquad (2)$$

where $E_{D/NiO}$ is the energy of the combined system, E_D is the energy of the single dye molecule, and the E_{NiO} is the energy of the NiO (100) surface.

3. RESULTS AND DISCUSSION

Free dye molecules. The molecular orbitals of the free dyes were examined to gain understanding on the intramolecular excitations for the charge transfer processes. The UV–Vis

177 spectra of the dye molecules are presented in Fig. 4 and the corresponding excitations in Table 1.
178 The calculated gaps between the highest occupied molecular orbital (HOMO) and the lowest
179 unoccupied molecular orbital (LUMO), i.e. the HOMO–LUMO gaps of the dyes are 2.5 eV for
180 **1**, 1.9 eV for **2**, 1.8 eV for **3**, and 1.9 eV for **4**. The strongest transitions take place in all dyes at
181 490–535 nm. Dye **1** has another strong transition at 395 nm which is at the border of the UV
182 light. The absorptions and excitations support the previous spectroscopic studies [17]: the first
183 excitation takes place inside the donor of the p-type D–A dye, i.e. inside TPA in **1** and inside
184 PMI in **2–4** and, and electron transfers to the acceptor moiety of the dye, i.e. to the LUMO level
185 of the acceptor in all dyes studied. Only **1** has one strong transition solely inside the acceptor,
186 which is from HOMO–1 to LUMO. In this case, the excited state can relax back to the ground
187 state, and if the relaxation is fast, it prevents the electron from transferring to the electrolyte. The
188 excitations are depicted using molecular orbital images in ESI, Fig. S2–S5.

189

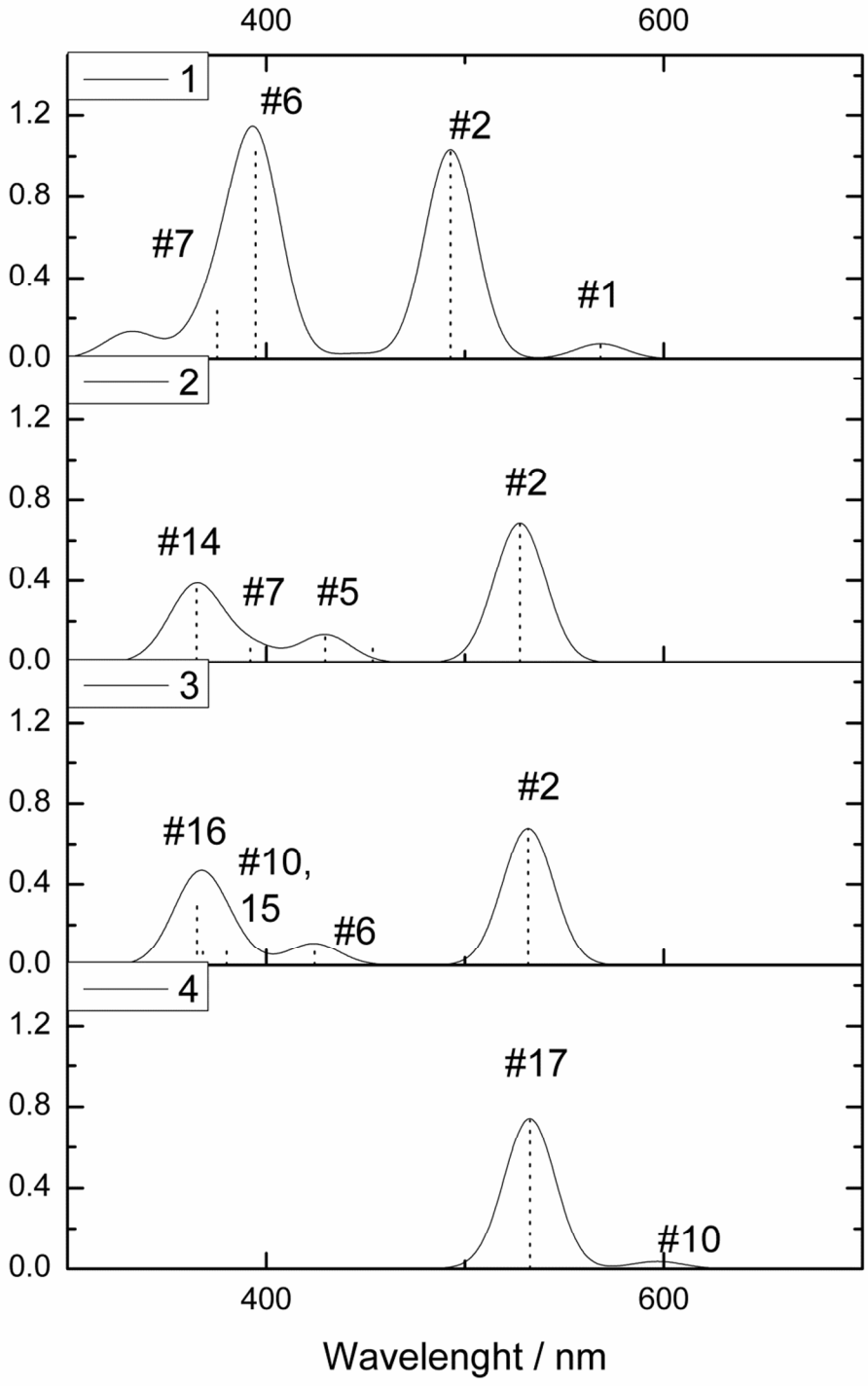

Fig. 4. UV–Vis spectra of **1**–**4**. Numbers corresponding to the excitations are presented in Table 1. Gaussian broadening of 30 nm bandwidth at ½ of the maximum height was used in spectra

193 **Table 1.** Excitations of the free dye molecules, type of the strongest excitations and the
194 corresponding absorption wavelengths, λ, oscillator strengths, f, and the percentages of the
195 contributing orbitals

Model	Excitation	Orbital	Type	λ / nm	f	%
1						
	1	HOMO-2 → LUMO		568	0.1	3
		HOMO → LUMO				96
	2	HOMO-1 → LUMO	A to A*	493	1.0	98
	6	HOMO → LUMO+1	D to D	395	1.1	95
	7	HOMO → LUMO+2		375	0.2	96
2						
	1	HOMO → LUMO		768	0.0	100
	2	HOMO → LUMO+1	D to D	528	0.7	99
	5	HOMO-1 → LUMO+1		430	0.1	97
	7	HOMO-2 → LUMO+1		392	0.1	98
	14	HOMO-6 → LUMO		365	0.2	80
3						
	1	HOMO → LUMO		771	0.0	100
	2	HOMO → LUMO+1	D to D	532	0.7	99
	6	HOMO-1 →LUMO+1		424	0.1	97
	10	HOMO-1 → LUMO+1		380	0.1	94
	15	HOMO-3 → LUMO+1		368	0.1	24
		HOMO → LUMO+3				38
	16	HOMO-9 → LUMO		365	0.3	91
4						
	1	HOMO-1 → LUMO		982	0.0	5
		HOMO → LUMO				94
	10	HOMO-5 → LUMO		596	<0.1	89
	17	HOMO-1 → LUMO+3	D to D	534	0.7	95

196 *A means an acceptor and D means a donor moiety of the molecule

197

198

199

The DOSs of the periodic dye **1**–**4** models without surface, calculated with DFT using CRYSTAL09, are illustrated in Fig. 5. The HOMO–LUMO gaps of the models **1**–**4**, are 2.5 eV, 1.8 eV, 1.7 eV and 1.8 eV, respectively. The DOSs demonstrate that the valence orbitals create strong, sharp peaks, which is typical for free molecules containing localized orbitals. The strong sharp peaks also indicate that the molecular orbitals of the dye are not interacting with their periodic images.

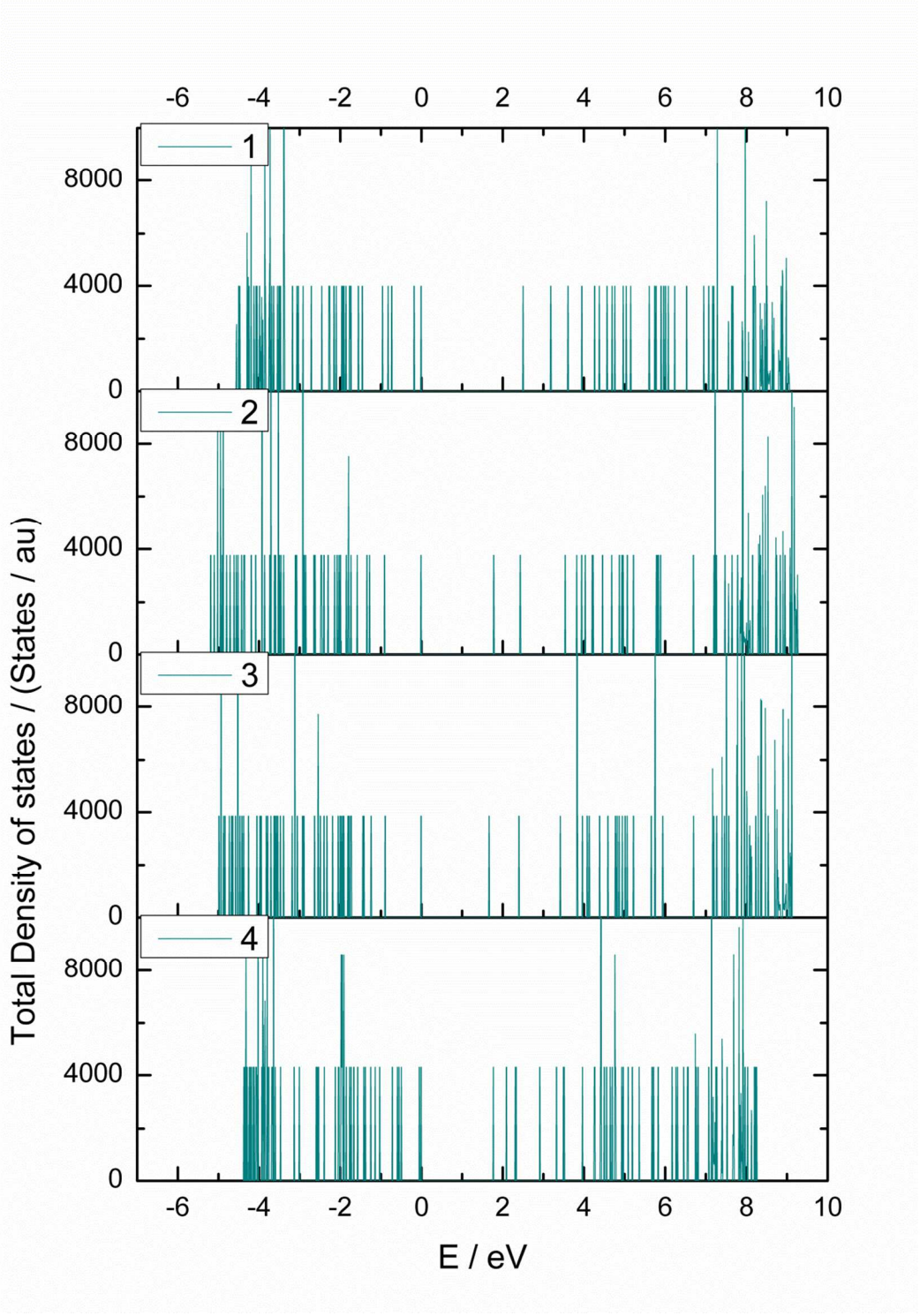

Fig. 5. Total "DOSs" (orbital energies) for periodic dye **1**–**4** models. Because the models are molecules in periodic boundary conditions, a set of sharp peaks are observed. Higher peaks are due to several orbitals being close in energy.

Semiconductor. Our optimized NiO bulk model has a lattice constant, a_0, of 4.213 Å and an indirect band gap of 4.5 eV. The effective mass, m^*, of the hole calculated from the band structure using equation (1) is 1.2. The indirect band gap of the NiO surface model is 4.0 eV and the effective mass of the hole is 0.6. This means that the surface conductivity is higher than the bulk conductivity. Further results of the bulk and surface including the band structure and the DOSs are presented and discussed in ESI.

Dye molecule adsorbed on the surface. The geometries of the combined dye-surface models are presented in Fig. 3. The geometries of the dyes **1** and **2** on the NiO (100) surface are relaxed. The dye **1** (Fig. 3) is able to chemisorb either via one **1a** or two **1b** different carboxylic acid groups and prefers an upright position on the surface. The dye **2** tilts towards the NiO (100) surface. The adsorption energies are given in Table 2. The shortest distance between two dye molecules is 2.5 Å, meaning the neighboring molecules can interact. The interaction may affect the adsorption energies and explain the differences between systems **1a** and **1b** (Table 2). The geometries of the dyes **3** and **4** were more challenging to optimize due to their structures, i.e. the phenyl linker between the donor and the acceptor in **3**, and the large fullerene acceptor in **4**. However, we will infer some features for the expected behavior of the combined systems of **3** and **4** based on the results calculated for **2** on the NiO surface. This can be done, because the donor moiety is the same and the carboxyphenoxy anchor unit is the same in **2** and **3.** Moreover, the carboxyphenyl anchor unit in **4** is more rigid than the carboxyphenoxy anchor group in **2**. This is justifiable also because the distance between the donor moiety and the NiO surface is comparable in each of these systems. The tilting was also observed for the partially optimized structure of **3**, which is well-founded, because the angle is expected to be about the same due to the sp^3 hybridization of the ether oxygen in the carboxyphenoxy anchor. In the combined system of **4**, the phenyl group of the anchor unit, which is directly bound to the PMI donor, makes the structure straight due to the sp^2 hybridized aromatic carbon atoms It is possible for hydrogen bonds to occur in two possible ways in our models. In the first case the hydrogen from carboxyl group is dissociated and adsorbed on the surface near the dye molecule. In this case hydrogen bond between the surface hydrogen and carboxyl oxygen may form, C–O(–Ni)•••H(–O), where atoms in parenthesis belong to surface NiO. However, the hydrogen bond is possible only if the hydrogen will stay close to the adsorbed dye molecule. In our models, we chose to place hydrogen next to the molecule and observe a hydrogen bond of 2.3 Å. The second case applies

only to molecule **1a**. Dye molecule **1a** has two anchoring groups and one of them is pointing away from the surface because the dye molecule is tilted. It is possible to have a hydrogen bond between carboxyl oxygen and hexyl group (C=O•••H–C). The distance of this hydrogen bond is 3.1 Å.

Table 2. Adsorption energies (in eV) for models **1a**, **1b** and **2**.

	1a	**1b**	**2**
Adsorption energy	-4.1*	-2.8	-1.3

* Additional stabilization due to dye-dye interactions

Table 3. HOMO-LUMO gaps of free, periodic and surface dye models.

	1	**2**	**3**	**4**
free	2.5	1.9	1.8	1.9
periodic	2.5	1.8	1.7	1.8
surface	2.5(**1a**) / 2.4(**1b**)	1.7	N/A	N/A

The DOSs (Fig. 6) and the band structures (Fig. 7) were calculated for the dyes **1** and **2** chemisorbed on the four (4) layers thick NiO (100) surface slab. The band gaps of these combined systems are due to the frontier orbitals of the dyes being 2.5 eV for **1a,** 2.4 eV for **1b** and 1.7 eV for **2**. These are relatively close to the calculated HOMO–LUMO gaps of the free and periodical models which have been collected to **Table 3**. However, it can be seen that the adsorption can lower the HOMO–LUMO gap by 0.1–0.2 eV. Closer examination of energy levels of **1b** reveals that the HOMO moves 0.1 eV higher in energy and LUMO+1, located also at the donor part of the dye, moves down 0.5 eV in energy due to the binding mode. Moreover, the NiO band gap drops from 4.06 eV to 3.96 eV, if chemisorption takes place through single anchoring group and to 3.90 eV if it takes place through two groups. Transitions that are expected for these systems are presented in Fig. 7. The calculated effective hole mass, m^*, is 0.7 for both **1** and **2** on the NiO (100) surface. Because the calculated m^* is 1.2 for the NiO bulk and 0.6 for the NiO (100) surface, the surface conductivity for the combined system of **2** is higher than the bulk conductivity of NiO.

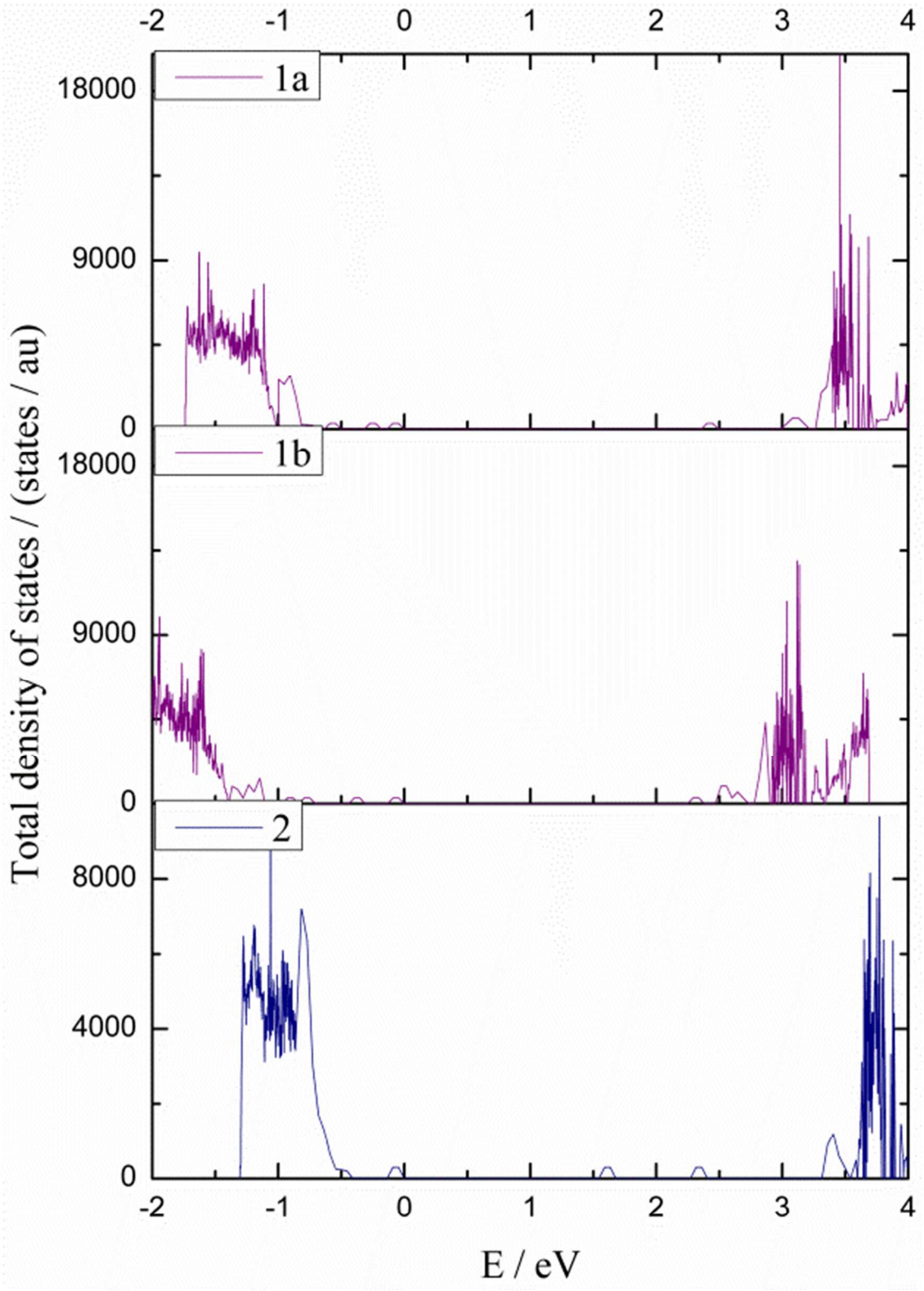

Fig. 6. DOS of the combined systems **1a**, **1b** and **2**.

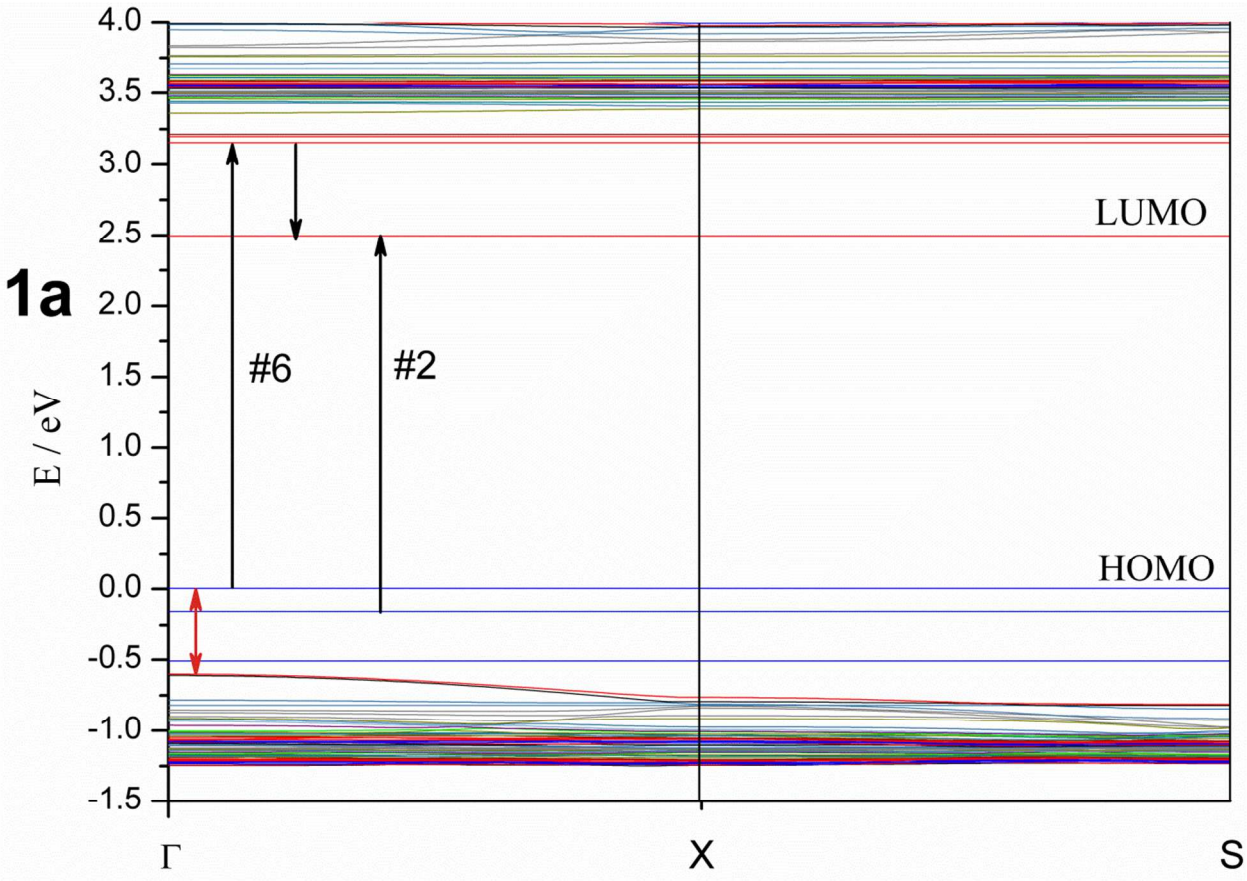

268

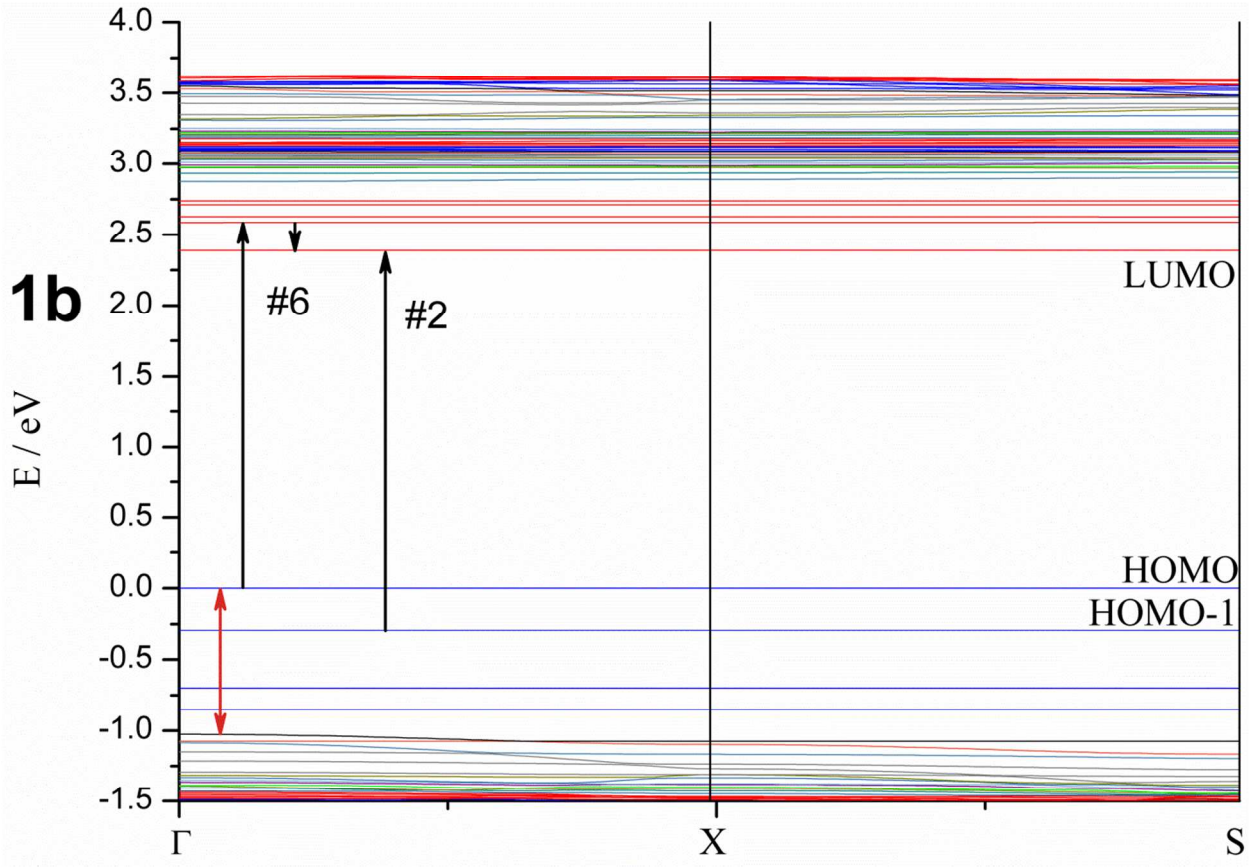

269

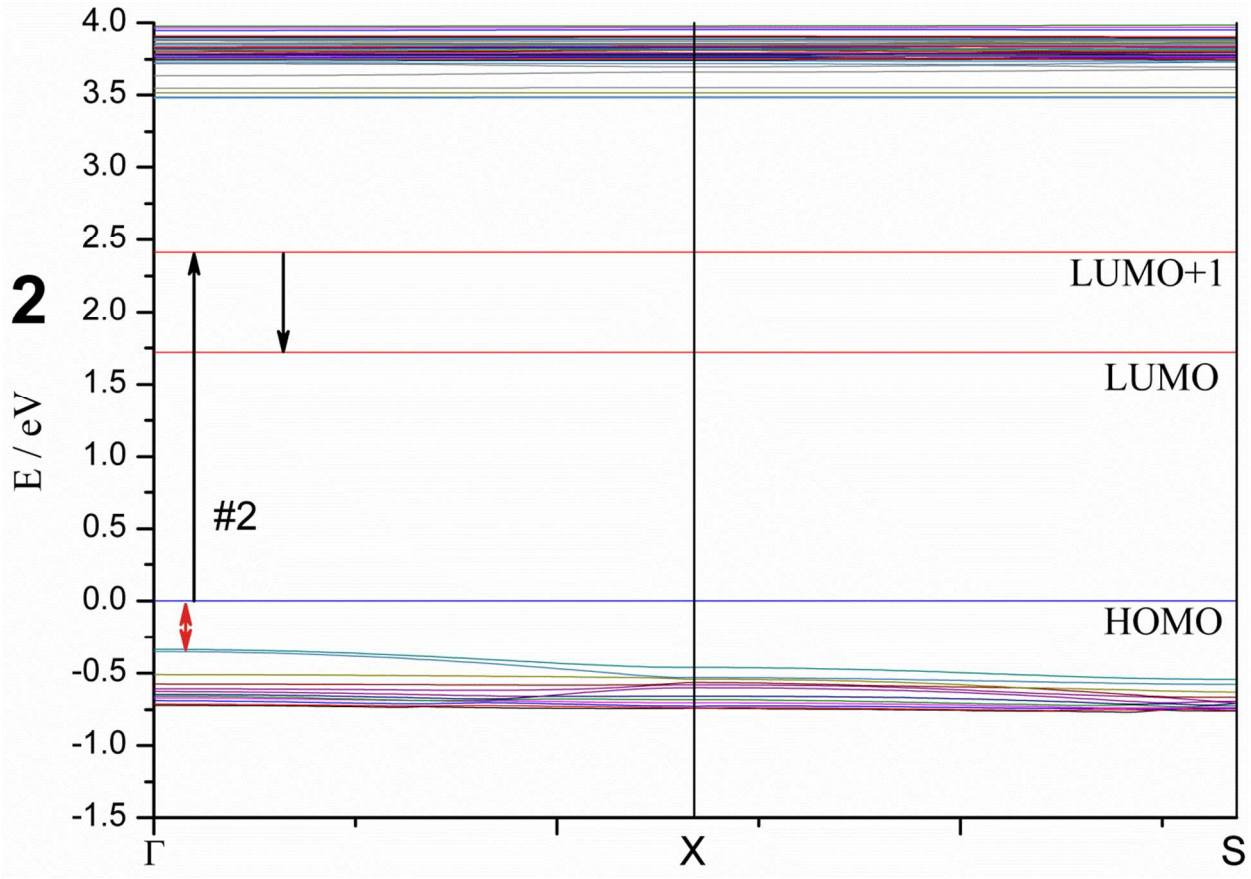

Fig. 7. Band structures of the combined models **1a**, **1b**, and **2**. The straight lines (blue for occupied, red for unoccupied) are for the molecule and the curved lines for the surface. Black arrows express the electronic excitations and relaxations in the dye molecule. The red arrow indicates the distance from the valence band of the NiO (100) surface to the HOMO of the dye molecule.

In the DOS and band calculations, the band gaps of the combined systems of **3** and **4** were not opening properly with the functional and the basis set applied, despite the usage of the gap widening tools, and we did not obtain a proper description of the electronic structures.

The band structure of the NiO (100) surface remains mostly the same whether it is covered with the dye or not, except for the shift in energy. Another difference is that the dispersion locates on the Γ point in the combined system and on the S point when there is no adsorbate on the NiO surface. Because the surface and the dye molecule interact only weakly, it is assumed that the

electronic transitions are similar to those predicted by the TDDFT calculations for the isolated dye molecules.

In all band structures **1a**, **1b** and **2** the HOMO is located above the valence band of the semiconductor, because we are using a perfect NiO model instead of p-type NiO with Ni-vacancies and high packing of the dye molecule. Both affect the energy level order between the surface and organic layer. Increase of NiO p-doping raises the VBM above dye HOMO level that is needed for driving the holes to NiO surface. Similar potential drop is needed for electrons to flow from dye to the electrolyte to complete the charge separation in dye-semiconductor junction. For this reason, we can compare the dye molecules relative to each other by looking at the energy difference between NiO valence band and dye HOMO level.

The calculated HOMO–LUMO gap of the dye **1** on the NiO (100) surface is 2.5 eV for the **1a** model and 2.4 eV for the **1b** model. The large gap makes the dye **1** ideal for collecting sunlight in a tandem device. The distance between the HOMO and conduction band is 0.60 eV in **1a** and 1.03 eV in **1b**. The HOMO–LUMO gap of 1.7 eV calculated for the dye **2** on the NiO (100) surface (Fig. 6 (DOS) and Fig. 7 (band)) is smaller than that of the dye **1**, making **2** less ideal for a p-type dye. The HOMO of the dye is located 0.34 eV above valence band, which is less than in the case of **1**. This means that it is located deeper in the valence band in the actual p-NiO and there is more driving force for charge transfer to the dye. Moreover, **2** is the smallest dye molecule that was investigated on the NiO surface in this paper, and therefore all of the structural parts of the combined system (the donor, the acceptor, and the surface) are close together which may make it easier for the charge transfer from one part to another.

4. CONCLUSIONS

The minimum energy geometries, electronic structures and electronic excitations of four p-type perylenemonoimide-based D–A dyes were calculated using DFT and TDDFT. PMI acts as an acceptor in **1** and as a donor in **2-4**. The DOSs and band structures were calculated for the free dyes, the NiO bulk, and the NiO (100) surface and for the dyes **1** and **2** on the NiO (100) surface.

Dyes adsorbed on the surface can be in either upright position (**1b**, **2**, **4**) or tilted (**1a**, **3**), depending on the geometry of the anchor and binding mode. The adsorption slightly lowers the NiO band gap, from 4.06 eV to 3.90–3.96 eV, and dye molecule band gaps by 0.1–0.2 eV.

Additionally, the adsorption mode in dye **1b** moves the LUMO+1 level down by 0.5 eV. The calculated effective mass of the hole, 1.2 for bulk, 0.6 for surface and 0.7 for combined models, indicates that in all cases the surface conductivity is higher than of the bulk.

The band structures of combined models **1a**, **1b** and **2** revealed that the binding mode in **1** affects the HOMO position by 0.5 eV. However, the model **2** has the lowest HOMO level compared to the pristine NiO, which means that the HOMO level is located deeper in the valence band in the actual p-NiO and is expected to have the highest driving force for charge transfer to p-NiO. Moreover, **2** is the smallest dye molecule that was investigated on the NiO surface in this paper, and therefore all of the structural parts of the combined system (the donor, the acceptor, and the surface) are close together which may make it easier for the charge transfer from one part to another. Also, it should be noted that the relative ordering of the dye HOMO and the NiO VBM can be changed and tuned by NiO doping.

Our next goal is to create a more accurate p-NiO model containing Ni vacancies and to use novel functionals such as GLLB-SC for more accurate analysis of the electronic structures.

ACKNOWLEDGEMENTS

Computing resources provided by the CSC - IT Center for Science Ltd, administrated by the Finnish Ministry of Education, are gratefully acknowledged. Funding received from the Academy of Finland and grants received from Walter Ahlström Foundation and Finnish Chemical Societies are greatly appreciated.

REFERENCES

1. N. Agnihotri, J. Photochem. Photobiol., 2014, 18, 18.

2. F. Odobel, L. Le Pleux, Y. Pellegrin, E. Blart, Accounts Chem. Res., 2010, 43, 8, 1063.

3. F. Odobel, Y. Pellegrin, J. Phys. Chem. Lett., 2013, 4, 2551.

4. B. O'Regan, M. Grätzel, Nature, 1991, 353, 737.

338 5. A. Yella, H.-W. Lee, H. N. Tsao, C. Yi, A. K. Chandiran, M. Nazeerudin, E. W. - G. Diau, C. - Y. Yeh, S. M. Zakeeruddin, M. Grätzel,
339 Science, 2011, 334, 629.

340 6. S. Mathew, A. Yella, P. Gao, R. Humphry-Baker, B. F. E. Curchod, N. Ashari-Astani, I. Tavernelli, U. Rothlisberger, Md. K.
341 Nazeeruddin, M. Grätzel, Nat. Chem., 2014, 6, 242.

342 7. F. Odobel, Y. Pellegrin, E.A. Gibson, A. Hagfeldt, A. L. Smeigh, L. Hammarström, Coord. Chem. Rev., 2012, 256, 2414.

343 8. A. Nattestad, A. J. Mozer, M. K. R. Ficher, Y. B. Cheng, A. Mishra, P. Bäuerle, U. Bach, Nat. Mater., 2010, 9, 31.

344 9. I. R. Perera, T. Daeneke, S. Makuta, Z. Yu, Y. Tachibana, A. Mishra, P. Bäuerle, C. A. Ohlin, U. Bach, L. Spiccia, Angew. Chem.
345 Int. Ed., 2015, 54, 3758.

346 10. W. Shockley, H. J. Queisser, J. Appl. Phys., 1961, 32, 510.

347 11. R. Swanson, Approaching the 29% limit efficiency of silicon solar cells, in: 31th PVSC, Orlando, Florida, 2005.

348 12. A. Nakasaka, H. Usami, S. Sumikura, S. Hasegawa, T. Koyama, E. Suzuki, Chem. Lett., 2005, 34, 4, 500.

349 13. J. He, H. Lindström, A. Hagfeldt,S. E. Lindquist, Sol. Energy Mat. Sol. Cells, 2000, 62, 265.

350 14. E. A. Gibson, A. L. Smeigh, L. L. Pleux, J. Fortage, G. Boschloo, E. Blart, Y. Pellegrin, F. Odobel, A. Hagfeldt, L. Hammarstöm,
351 Angew. Chem, Int. Ed., 2009, 48, 4402.

352 15. A. Morandeira, J. Fortage, L. Edvinsson, L. Le Pleux, E. Blart, G. Boschloo, A. Hagfeldt, L. Hammarström, F. Odobel, J. Phys.
353 Chem.C., 2008, 112, 1721.

354 16. S. Mori, S. Fukuda, S. Sumikura, Y. Takeda, Y. Tamaki, E. Suzuki, T. Abe, J. Phys. Chem. C., 2008, 112, 16134.

355 17. L. Le Pleux, A. L. Smeigh, E. Gibson, Y. Pellegrin, E. Blart, G. Boschloo, A. Hagfeldt, L. Hammarström, F. Odobel, Energy
356 Environ. Sci., 2011, 4, 2075.

357 18. D. Niedzialek, I. Duchemin, T. B. de Queiroz, S. Osella, A. Rao, R. Friend, X. Blasé, S. Kümmel, D. Beljonne, Adv. Funct. Mat.,
358 2015, 25, 13, 1972.

359 19. S. Sumikura, S. Mori, S. Shimizu, U. Hisanao, E. Suzuki, J. Photochem. Photobiol. A, 2008, 194, 143.

360 20. A. Nattestad, X. Zhang, U. Bach, Y.-B. Cheng. J. Photonics Energy, 2011, 1, 011103-1.

21. M. Yu, G. Natu, Z. Ji, Y. Wu, J. Phys. Chem. Lett., 2012, 3, 1074.

22. S. Powar, T. Daeneke, M. T. Ma, D. Fu, N. W. Duffy, G. Götz, M. Weidelener, A. Mishra, P. Bäuerle, L. Spiccia, U. Bach, Angew. Chem. Int. Ed., 2013, 52, 602.

23. X. H. Chan, J. R. Jennings, M. A. Hossain, K. K. Z. Yu, Q, Wang, J. Electrochem. Soc., 2011, 158, 7, H733.

24. A. B. Munõz-García, M. Pavone, Phys. Chem. Chem. Phys., 2015, 17, 12238.

25. A. Maufroy,L Favereau, F. B. Anne, Y. Pellegrin, E. Blart, E. Blart, M. Hissler, D. Jacquemin, F. Odobel, J. Mat. Chem. A, 2015, 3, 3908.

26. L. Favereau, J. Warnan, Y. Pellegrin, E. Blart, M. Boujtita, D. Jacquemin, F. Odobel, Chem. Commun., 2013, 49, 8018.

27. Y. Pellegrin, L. Le Pleux, E. Blart, A. Renaud, B. Chavillon, N. Szuwarski, M. Boujtita, L. Cario, S. Jobic, D. Jacquemin, F. Odobel, J. Photochem. Photobiol. A, 2011, 219, 235.

28. G. A. Sawatzky, J. W. Allen. Phys. Rev. Lett., 1984, 53, 2339.

29. K. Terakura, A. R. Williams, T. Oguchi, J. Kübler, Phys. Rev. B., 1984, 30, 8, 4734.

30. D. Alders, L. H. Tjeng, F. C. Voogt, T. Hibman, G. A. Sawatzky, C. T. Chen, J. Vogel, M. Sacchi, S. Iacobucci, Phys. Rev. B., 1998, 57, 18, 623.

31. V.E. Henrich and P.A. Cox, The Surface Science of Metal Oxides (Cambridge Univ. Press, NY, 1994.

32. Gaussian 09, Revision D.01, M. J. Frisch, G. W. Trucks, H. B. Schlegel, G. E. Scuseria, M. A. Robb, J. R. Cheeseman, G. Scalmani, V. Barone, B. Mennucci, G. A. Petersson, H. Nakatsuji, M. Caricato, X. Li, H. P. Hratchian, A. F. Izmaylov, J. Bloino, G. Zheng, J. L. Sonnenberg, M. Hada, M. Ehara, K. Toyota, R. Fukuda, J. Hasegawa, M. Ishida, T. Nakajima, Y. Honda, O. Kitao, H. Nakai, T. Vreven, J. A. Montgomery, Jr., J. E. Peralta, F. Ogliaro, M. Bearpark, J. J. Heyd, E. Brothers, K. N. Kudin, V. N. Staroverov, R. Kobayashi, J. Normand, K. Raghavachari, A. Rendell, J. C. Burant, S. S. Iyengar, J. Tomasi, M. Cossi, N. Rega, J. M. Millam, M. Klene, J. E. Knox, J. B. Cross, V. Bakken, C. Adamo, J. Jaramillo, R. Gomperts, R. E. Stratmann, O. Yazyev, A. J. Austin, R. Cammi, C. Pomelli, J. W. Ochterski, R. L. Martin, K. Morokuma, V. G. Zakrzewski, G. A. Voth, P. Salvador, J. J. Dannenberg, S. Dapprich, A. D. Daniels, Ö. Farkas, J. B. Foresman, J. V. Ortiz, J. Cioslowski, and D. J. Fox, Gaussian, Inc., Wallingford CT, 2009.

33. A. D. Becke, J. Chem. Phys., 1993, 98, 5648.

34. C. Lee, W. Yang, R. G. Parr, Phys. Rev. B., 1988, 37, 2, 785.

386 35. P. J. Stephens, F. J. Devlin, C. F. Chabalowski, M. J. Frisch, J. Phys. Chem., 1994, 98, 11623.

387 36. R. Dovesi, R. Orlando, B. Civalleri, C. Roetti, V. R. Saunders and C. M. Zicovich-Wilson, CRYSTAL: a computational tool for the
388 ab initio study of the electronic properties of crystals, Z. Kristallogr., 2005, 220, 571.

389 37. R. Dovesi, V. R. Saunders, C. Roetti, R. Orlando, C. M. Zicovich-Wilson, F. Pascale, B. Civalleri, K. Doll, N. M. Harrison, I. J.
390 Bush, P. D'Arco and M. Llunell, CRYSTAL09, CRYSTAL09 User's Manual, University of Torino, Torino, 2009.

391 38. M. F. Peintinger, D.Vilela Oliveira, T. Bredow, J. Comp. Chem., 2013, 34, 451.

392 39. C. Gatti, V.R. Saunders, C. Roetti, J. Chem. Phys., 1994, 101, 10686.

393 40. M.D. Towler, N.L. Allan, N.M. Harrison, V.R. Saunders, W.C. Mackrodt, E. Apra, Phys. Rev. B., 1994, 50, 5041.

394 41. S. Choi, K. Koumoto, H. Yanagida, J. Mater. Sci., 1986, 21, 1947.